On Poisson Compressed Sensing and Parameter Estimation in Sheet-of-Light Surface Scanning

Sutharshun Varatharaajan*, Florian Römer*, Günther Kostka†, Fabian Keil†, Franz Uhrmann†, Giovanni Del Galdo*
*Digital Broadcasting Laboratory, Technische Universität Ilmenau, Germany
†Fraunhofer Institute for Integrated Circuits IIS, Fuerth, Germany

***Abstract*—Compressed Sensing (CS) has been successfully applied in a number of imaging systems since it can fundamentally increase frame rates and/or the resolution. In this paper, we apply CS to 3-D surface acquisition using Sheet-of-Light (SOL) scanning. The application of CS could potentially increase the speed of the measurement and/or enhance scan resolution with fewer measurements. To analyze the potential performance of a CS-SOL system, we formulate the estimation of the height profile of a target object as a compressive parameter estimation problem and investigate the achievable estimation accuracy in the presence of noise. In the context of compressed sensing, measurement models with AWGN are typically analyzed. However, in imaging applications there are multiple noise sources giving rise to different statistical noise models in which Poisson noise can be the dominating noise source. This is particularly true for photon-counting detectors that are used in low light settings. Therefore, in this paper we focus on the compressive parameter estimation problem in presence of Poisson distributed photon noise. The achievable estimation accuracy in obtaining height profiles from compressed observations is systematically analyzed with the help of the Cramer-Rao Lower Bound (CRLB). This analysis allows us to compare different CS measurement strategies and quantify the parameter estimation accuracy as a function of system parameters such as the compression ratio, exposure time, image size, etc.**

I. Introduction

Compressive Sensing (CS) improves the efficiency of signal measurements compared to conventional Nyquist sampling by combining the measurement and compression stages [1]. CS establishes that it is possible to sample a signal below its mandated Nyquist rate and still recover it completely, given that the signal has an underlying structure [2]. The applications of CS have been identified in medical imaging, distributed sensor networks, radar imaging, cognitive radio and parameter estimation problems [3], among others. The reduction in the required number of measurements can lead to faster acquisition of measurements and/or cheaper sensors without significant loss in reconstruction quality.

Sheet-of-Light (SOL) surface scanning is used in a wide range of applications such as quality control in production/assembly lines [4], [5], robotic vision and navigation [6], underwater scanning [7], terrestrial scanning [8], and water level profile estimation [9]. It is a technology that could benefit from CS implementations in overcoming its speed and resolution bottlenecks. The laser intensity image recorded in SOL scanners is inherently sparse and it also has a sparse representation in a dictionary which can be derived from the incident laser intensity spread function. The reduction in the number of sensor readouts due to certain CS implementations like coded aperture sensors [10] or CMOS imagers [11] (see also [12] and references therein) could help in obtaining higher frame rates and/or a higher resolution in the scanning process.

In this paper, we discuss how CS can be applied to SOL. We show that the acquisition of the height profile from compressed measurements can be modeled as a compressive parameter estimation problem. We analyze the achievable accuracy in the presence of noise using Cramer-Rao Lower Bounds (CRLBs). In particular, we focus on Poisson noise which occurs in image sensors (particularly in low-light conditions) and is much less investigated than the more common additive white Gaussian noise (AWGN). The derived CRLBs for Poisson noise allow us to compare alternative compressive measurement strategies and to study the impact of system parameters on the height profile estimation quality.

This paper is structured as follows. In Section II we introduce the data model and the underlying parameter estimation problem. Section III introduces the Poisson measurement model and its implications on the compressive measurement. The CRLBs are derived and analyzed in Section IV before drawing conclusions in Section V.

II. Data Model and Problem Formulation

A. SOL measurement setup and data model

The experimental setup in a sheet-of-light laser scanner is shown in Fig.

In essence, every column of the image contains a sampled, shifted version of the original laser intensity shape where the shift depends on the height of the object's surface and is the value of interest. Hence, in the absence of deterministic distortions due to object height variations (i.e., considering that we sense a relatively smooth object that does not distort the shape of the intensity spread captured), the measured discrete intensity spread can be considered translation-invariant [13]. Therefore, a manifold model can be considered for compact representation of the captured laser intensity [14].

Considering that a cross section of the incident laser line has an intensity spread $G(t)$, where t is position, we represent the N samples from a shifted version of the function $G(t-\mu)$ at the points $t = 0, 1, \ldots, N-1$ by the vector $\boldsymbol{g}(\mu) \in \mathbb{R}_+^N$. The

This work was partially supported by the Carl-Zeiss Foundation under the postdoctoral scholarship project "EMBiCoS".

978-0-9928-6265-7/16/$31.00 ©2016 IEEE

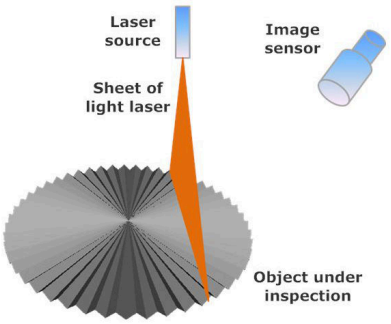

Fig. 1. Scene of sheet-of-light laser scanning

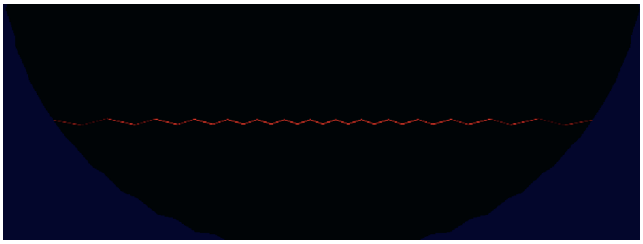

Fig. 2. A laser projection scene recorded by the sensor

image captured by the sensors, $\boldsymbol{S}(\boldsymbol{c},\boldsymbol{\mu}) \in \mathbb{R}_{+}^{N\times L}$, consists of the sampled intensity spread function with varying shifts depending on the object height at the point where the laser is projected. Without considering any distortions, the image obtained can be written as

$$\begin{aligned}\boldsymbol{S}(\boldsymbol{c},\boldsymbol{\mu}) &= [c_1\,\boldsymbol{g}(\mu_1)\;\; c_2\,\boldsymbol{g}(\mu_2)\;\; \ldots\;\; c_L\,\boldsymbol{g}(\mu_L)] \\ &= [\boldsymbol{s}(c_1,\mu_1)\;\boldsymbol{s}(c_2,\mu_2)\;\ldots\;\boldsymbol{s}(c_L,\mu_L)] \end{aligned} \quad (1)$$

where $\boldsymbol{\mu} = [\mu_1\;\mu_2\;\ldots\;\mu_L]^T$ are the translation parameters (laser peak positions) to be estimated. The varying amplitude parameters $\boldsymbol{c} = [c_1\;c_2\;\ldots\;c_L]^T$ are partly due to height variations in the object scanned and they need not be estimated. The vector $\boldsymbol{g}(\mu)$, for various values of the parameter μ, traces a 1-D manifold $\Gamma_{\boldsymbol{g}} = \{\boldsymbol{g}(\mu) : \mu \in [0, N-1]\} \subset \mathbb{R}^N$. In practice, the image sensor is positioned in such a way that the laser line in the image captured is well within the image periphery and hence, the intensity profile is captured completely. Hence, only a subset of the possible parameter values are practically viable.

It is obvious from (that the estimation of the parameters $\boldsymbol{\mu}$ can be carried out for each column separately since each parameter μ_ℓ influences only the measurements in the same column $\boldsymbol{s}_\ell$. This is advantageous since the L separate parameter estimation problems can be solved in parallel and since each of them is equivalent to a simple peak finding problem. For the latter, there exist numerous efficient methods, e.g., Center of Gravity, Gaussian Approximation, Parabolic Fitting, cf. [15] for a survey.

B. Application of CS to SOL

The sparsity of the observed image as well as its manifold representation introduced in (suggests that the measurements can be significantly compressed without substantial loss of information. In the absence of noise, a set of compressive measurements of an image can be written as

$$\boldsymbol{y} = \boldsymbol{\Phi}\,\mathrm{vec}\{\boldsymbol{S}(\boldsymbol{c},\boldsymbol{\mu})\}. \quad (2)$$

CS-based imaging systems typically advocate measurements according to (where $\boldsymbol{\Phi}$ is a full matrix, which implies mixing of pixels from all over the image in order to make every measurement as informative as possible [12]. Applying (to SOL would destroy the separability of the parameter estimation problems per column as explained in Section

The capability of obtaining the two modes of measurements differs according to the sensor we are trying to implement. The digital micromirror array patterns in the single pixel camera [16] can be configured to obtain measurements in either the ICM or MCM mode. The coded aperture CS sensors [10], on the other hand, can only measure the image as a whole and cannot measure each column independently.

III. Poisson Compressed Sensing in Sheet-of-Light Laser Scanning

A. Poisson noise in image sensors

In any modern image sensors, we have to consider a variety of noise sources. While some of them (such as, amplifier noise, KTC noise, and on-chip electronic noise) give rise to additive white Gaussian noise (AWGN), there are many others that are best described by Poisson random processes, e.g., photon noise, quantization noise and thermal noise [17]. In this paper, we focus on Poisson noise, for two reasons. Firstly, while AWGN measurement models in CS are well investigated, Poisson noise is rarely discussed in the state of the art. This may be due to the fact that among the many applications of CS, imaging is the one of the very few where Poisson noise is relevant. Moreover, even in imaging this fact is often ignored (notable exceptions include [18], [19]). Secondly, AWGN distortions can be contained using proper electronic design as mentioned in [17] whereas Poisson distortions in low-light environments (originating from photon counting noise or scattering) are inevitable. Note that in many setups, to record only the laser light in the camera, analog filters are used in front of the camera aperture or the measurements are made in a dark environment. In such scenarios, Poisson distributed photon noise dominates the image distortions. Hence, the study of image measurements with Poisson distortions in SOL scanners is vital and of higher importance.

Considering the photon count from a single pixel, $x \in \mathbb{Z}_+$, we can write

$$x \sim \mathrm{Poisson}(\lambda T)\,, \quad (3)$$

where λ is the intensity per unit time and T is the exposure time, i.e., the duration over which photons are collected. The above equation means that the photon count x follows a Poisson distribution with mean λT (always non-negative), which is its variance as well. As we can see, Poisson noise is neither additive nor independent from the signal like additive

white Gaussian noise. The probability density function of x is given by,

$$\Pr[X = x] = \begin{cases} \frac{e^{-\lambda T}\cdot(\lambda T)^x}{x!} & \lambda T > 0 \\ \delta(x) & \lambda T = 0 \end{cases}, X \in \mathbb{Z}_+ . \quad (4)$$

According to [17], the SNR of the measurement can be expressed as

$$\rho = \frac{(\mathbb{E}(x))^2}{\mathbb{E}(x^2) - (\mathbb{E}(x))^2} = \lambda T . \quad (5)$$

Therefore, we have that the SNR and the signal's variance increase at the same rate. This means that even though the variance of the photon count increases with the average number of incident photons, the SNR increases as well, which means that we expect higher fidelity in the measurements with increasing average photon count (which corresponds to increasing intensity rate or exposure time).

B. Poisson Compressed Sensing

The fact that the sensors are modeled as photon counters has implications on the mathematical model of the compressive measurement strategies.

In the case of SOL scanners with CS, the compressive Poisson measurements $\boldsymbol{y} \in \mathbb{Z}_+^{M\times 1}$ can be modeled as,

$$\boldsymbol{y} \sim \text{Poisson}(\boldsymbol{\Phi}\,\text{vec}\{\boldsymbol{S}(\boldsymbol{c},\boldsymbol{\mu})\}) . \quad (6)$$

The expression indicates that the k-th photon count, y_k, $k = 1, 2, \ldots, M$, follows a Poisson distribution with its mean being the k-th coefficient of the vector $\boldsymbol{\Phi}\,\text{vec}\{\boldsymbol{S}(\boldsymbol{c},\boldsymbol{\mu})\}$. To relate the intensity rate λ and the exposure time T from the Poisson model in (to (, we consider their product which can be interpreted as the reflected intensity (in units of photons) at the peak of the profile $G(t)$. We carry out the analysis in terms of the intensities $\boldsymbol{c}$. In practice, in order to increase the value of $\boldsymbol{c}$ we can either increase the intensity rate of the measurements λ (using, e.g., a brighter laser source) or the exposure time T.

As discussed in [18], the measurement kernel $\boldsymbol{\Phi}$ should satisfy some physical constraints to be a realizable optical system, i.e.,

- *Positivity*: The product of the measurement matrix $\boldsymbol{\Phi}$ and the signal (the laser intensity image) should produce a vector with only non-negative coefficients, given that the signal is non-negative, i.e.,

$$\text{vec}\{\boldsymbol{S}(\boldsymbol{c},\boldsymbol{\mu})\} \succeq \boldsymbol{0}_{NL\times 1} \implies \boldsymbol{\Phi}\,\text{vec}\{\boldsymbol{S}(\boldsymbol{c},\boldsymbol{\mu})\} \succeq \boldsymbol{0}_{M\times 1} , \quad (7)$$

  where the symbol $\succeq$ represents an element-wise comparison and $\boldsymbol{0}$ represents a zero matrix with its size mentioned in the suffix.
- *Flux preservation*: The mean total intensity captured should not exceed the total intensity incident on the object. Mathematically, we can write it as

$$\sum_{m=1}^{M} (\boldsymbol{\Phi}\,\text{vec}\{\boldsymbol{S}(\boldsymbol{c},\boldsymbol{\mu})\})_m \leq \sum_{n=1}^{NL} (\text{vec}\{\boldsymbol{S}(\boldsymbol{c},\boldsymbol{\mu})\})_n , \quad (8)$$

  where $(.)_i$ denotes the i-th entry of the vector in the brackets.

Two types of matrices that satisfy the above constraints are dense pseudorandom matrices and the normalized adjacency matrix of an expander graph [18]. CS sensors that obtain optical projections of the scene sensed like the coded apertures [10] or the single pixel camera [16] can realize a Poisson CS system that complies with the constraints mentioned above.

IV. Cramér-Rao Lower Bound Analysis

In this section we derive the Cramér-Rao Lower Bound (CRLB) to assess the performance of three different mode of measurements - uncompressed, CS-ICM and CS-MCM in the presence of Poisson noise. We first discuss the CRLB of the uncompressed measurements. The measurements $\boldsymbol{x} \in \mathbb{Z}_+^{NL\times 1}$ in this case are modeled as,

$$\boldsymbol{x} \sim \text{Poisson}(\text{vec}\{\boldsymbol{S}(\boldsymbol{c},\boldsymbol{\mu})\}) . \quad (9)$$

To compute the Fisher information matrix, we need to consider all the parameters that influence the distribution of the observations, which are the desired parameters $\boldsymbol{\mu}$ as well as the amplitudes $\boldsymbol{c}$ which act as nuisance parameters. Therefore, the set of parameters involved in the estimation process is $\boldsymbol{\tau} = [\boldsymbol{c}^T \boldsymbol{\mu}^T]^T \in \mathbb{R}^{2L\times 1}$. The (i,j)-th element of the Fisher information matrix $\boldsymbol{F}^{(\text{UC})} \in \mathbb{R}^{2L\times 2L}$ can then be obtained by evaluating

$$F_{i,j}^{(\text{UC})} = \text{E}_{\boldsymbol{x}} \left\{ \frac{\partial \log p_{\boldsymbol{x}|\boldsymbol{\tau}}(\boldsymbol{x})}{\partial \tau_i} \cdot \frac{\partial \log p_{\boldsymbol{x}|\boldsymbol{\tau}}(\boldsymbol{x})}{\partial \tau_j} \right\} , \quad (10)$$

where $p_{\boldsymbol{x}|\boldsymbol{\tau}}(\boldsymbol{x})$ is the PDF of the observations parametrized by $\boldsymbol{\tau}$. Inserting the Poisson distribution from (, it is easy to show that (can be written as

$$F_{i,j}^{(\text{UC})} = \left(\frac{\partial\,\text{vec}\{\boldsymbol{S}(\boldsymbol{c},\boldsymbol{\mu})\}}{\partial \tau_i} \right)^T \boldsymbol{\Theta}_{\text{UC}}^{-1} \left(\frac{\partial\,\text{vec}\{\boldsymbol{S}(\boldsymbol{c},\boldsymbol{\mu})\}}{\partial \tau_j} \right) , \quad (11)$$

where $\boldsymbol{\Theta}_{\text{UC}} = \text{diag}\{\text{vec}\{\boldsymbol{S}(\boldsymbol{c},\boldsymbol{\mu})\}\}$ is the covariance matrix of the measurements. The average CRLB per column is obtained from the Fisher matrix as follows

$$\mathbb{E}\left(\frac{1}{L} \|\boldsymbol{\mu} - \hat{\boldsymbol{\mu}}\|_2^2 \right) \geq \frac{1}{L} \text{trace}(\boldsymbol{A}^T (\boldsymbol{F}^{(\text{UC})}(\boldsymbol{\tau}))^{-1} \boldsymbol{A}) , \quad (12)$$

with $\hat{\boldsymbol{\mu}} \in \mathbb{R}^L$ being the estimate of the translation parameters and $\boldsymbol{A}^T = [\boldsymbol{0}_{L\times L}\ \boldsymbol{1}_{L\times L}]$.

In the case of CS, a similar derivation shows that the (i,j)-th coefficient of the Fisher matrix $\boldsymbol{F}^{(\text{CS})}(\boldsymbol{\tau}) \in \mathbb{R}^{2L\times 2L}$ is,

$$F_{i,j}^{(\text{CS})} = \left(\frac{\partial\,\boldsymbol{\Phi}\,\text{vec}\{\boldsymbol{S}(\boldsymbol{c},\boldsymbol{\mu})\}}{\partial \tau_i} \right)^T \boldsymbol{\Theta}_{\text{CS}}^{-1} \left(\frac{\partial\,\boldsymbol{\Phi}\,\text{vec}\{\boldsymbol{S}(\boldsymbol{c},\boldsymbol{\mu})\}}{\partial \tau_j} \right) , \quad (13)$$

with the covariance matrix $\boldsymbol{\Theta}_{\text{CS}} = \text{diag}\{\boldsymbol{\Phi}\text{vec}\{\boldsymbol{S}(\boldsymbol{c},\boldsymbol{\mu})\}\}$. The CRLB is computed with the same formula as (.

The entire Fisher information matrices can be computed via

$$\boldsymbol{F}^{(\text{UC})}(\boldsymbol{\tau}) = \boldsymbol{V}^T \boldsymbol{\Theta}_{\text{UC}}^{-1} \boldsymbol{V} , \quad (14)$$

$$\boldsymbol{F}^{(\text{CS})}(\boldsymbol{\tau}) = \boldsymbol{V}^T \boldsymbol{\Phi}^T \boldsymbol{\Theta}_{\text{CS}}^{-1} \boldsymbol{\Phi} \boldsymbol{V} . \quad (15)$$

where the matrix $\boldsymbol{V} \in \mathbb{R}^{NL \times 2L}$ has the following structure:

$$\boldsymbol{V} = \left[\boldsymbol{I}_L \diamond \boldsymbol{G}(\boldsymbol{\mu}), \quad \boldsymbol{I}_L \diamond \left(\dot{\boldsymbol{G}}(\boldsymbol{\mu}) \cdot \mathrm{diag}\{\boldsymbol{c}\} \right) \right] \tag{16}$$

where $\diamond$ denotes the Khatri-Rao (column-wise Kronecker) product, $\boldsymbol{G}(\boldsymbol{\mu}) = [\boldsymbol{g}(\mu_1), \ldots, \boldsymbol{g}(\mu_L)]$, $\dot{\boldsymbol{G}}(\boldsymbol{\mu}) = [\dot{\boldsymbol{g}}(\mu_1), \ldots, \dot{\boldsymbol{g}}(\mu_L)]$, and $\dot{\boldsymbol{g}}(\mu) = \frac{\mathrm{d}\boldsymbol{g}(\mu)}{\mathrm{d}\mu}$.

Using straightforward calculations, we can obtain simplified expressions for the CRLB for μ_ℓ. In the uncompressed case, we

$$\mathbb{E}\left(|\hat{\mu}_\ell - \mu_\ell|^2 \right) \geq \frac{1}{c_\ell} \cdot \frac{1}{\sum_{n=1}^{N} \frac{\dot{g}_n(\mu_\ell)^2}{g_n(\mu_\ell)} - \frac{\left(\sum_{n=1}^{N} \dot{g}_n(\mu_\ell)\right)^2}{\sum_{n=1}^{N} g_n(\mu_\ell)}}. \tag{17}$$

Moreover, for the ICM case, the closed-form expression looks like (with $\boldsymbol{g}(\mu)$ replaced by $\boldsymbol{\Phi}^{(\mathrm{c})} \cdot \boldsymbol{g}(\mu)$. Equation (is instructive because it shows the explicit dependence of the CRLB on the intensity c_ℓ as well as the pulse $\boldsymbol{g}(\mu)$ and its derivative $\dot{\boldsymbol{g}}(\mu)$.

V. Numerical results

In this section we present some numerical results to evaluate the achievable estimation accuracy as a function of all the system parameters, including the different modes of measurement (ICM, MCM). The simulations to obtain the CRLB plots are carried out for a Gaussian shaped incident intensity spread, where the n-th coefficient of the sampled intensity spread across the ℓ-th column ($\ell = 1, 2, \ldots, L$) of the laser intensity image $\boldsymbol{S}(\boldsymbol{c}, \boldsymbol{\mu}) \in \mathbb{R}_{+}^{N \times L}$ is given by,

$$S_{n,\ell} = c_\ell \cdot \exp\left(-\frac{(n - 1 - \mu_\ell)^2}{2\sigma^2} \right), \; n = 1, 2, \ldots, N\,. \tag{18}$$

The variable σ is used to control the width of the intensity spread function. The values chosen for N and σ are 50 and 1, respectively. The amplitude parameters $\boldsymbol{c}$ for all the columns are kept the same and they control the peak intensity of the measured scene. Dense pseudorandom matrices are used for the CS measurements in the experiment. In the experiment, for MCM, the entries of the matrix used are either 0 or $1/M$ with equal probability. In the case of ICM, block diagonal matrices are used, with each block containing either 0 or L/M with equal probability. The normalizing factors are different for ICM and MCM to have the same average number of incident photons per measurement, over several ensembles, for both cases.

The CRLB for varying values of compression ratios $\kappa = M/NL$ and L are plotted against the peak intensity c in Fig. Figure

VI. Conclusions

In this paper we discuss the application of Compressed Sensing (CS) to Sheet-of-Light (SOL) surface scanning. We discuss two CS measurement approaches, the independent column measurements (ICM) which preserve the separability of the underlying parameter estimation problem, as well as the mixed column measurements (MCM) which are inherent in

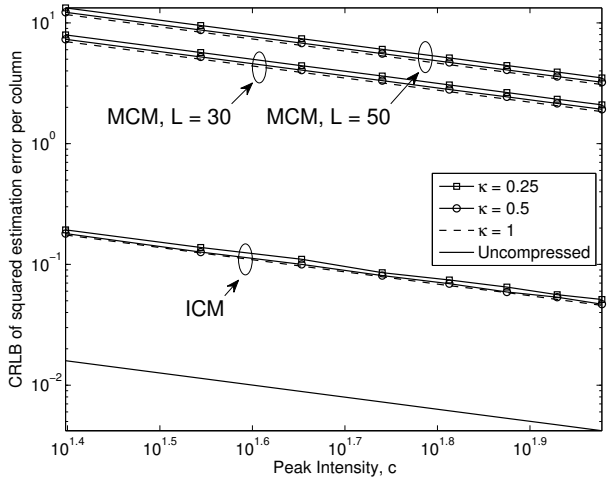

Fig. 3. CRLB of squared estimation error per column plotted against the peak intensity c for uncompressed measurements, CS-ICM and CS-MCM for varying values of L and κ.

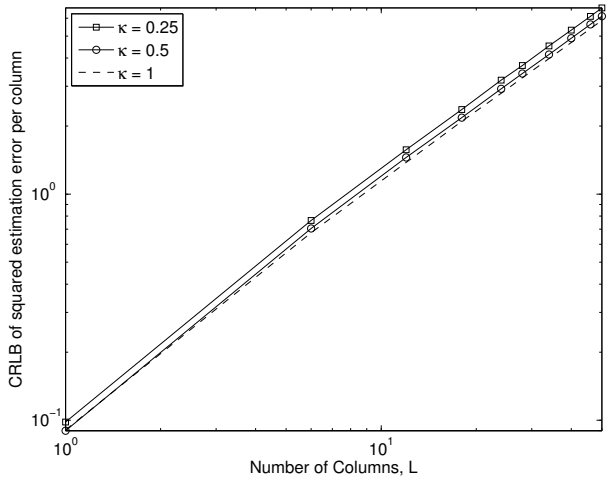

Fig. 4. CRLB of squared estimation error per column for CS-MCM plotted against the number of columns in the laser intensity image, L for varying values of the compression ratio, κ.

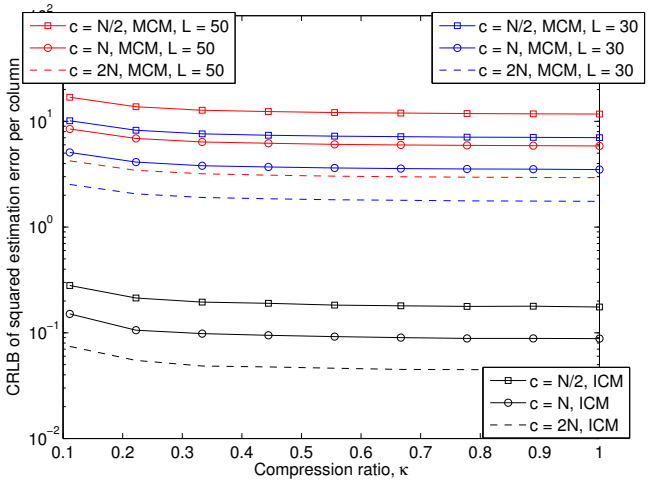

Fig. 5. CRLB of squared estimation error per column for Poisson ICM and MCM plotted against compression ratio κ for varying values of peak intensity c and number of columns in the image L.

some of the practical embodiments of CS. We compared these strategies in the presence of Poisson noise, which is commonly encountered in imaging systems and has not been discussed in conjunction with parameter estimation. In order to assess the achievable estimation accuracy, we have derived the Cramer-Rao Lower Bounds (CRLBs) for this setting. These also allow us to systematically study the influence of system parameters, such as the peak intensity, compression rate, image size, etc. Our analysis shows that ICM is superior to MCM but there is a degradation compared to the uncompressed case. This is partly due to the fact that the compressive measurements lead to a reduction in the total number of observed photons. However, these results are specific to the dense pseudo-random matrices that were considered in this paper.

Future work involves quantifying the performance degradation in CS analytically. Based on this analysis, more efficient measurement matrices can be devised.

REFERENCES

[1] D. Donoho, "Compressed Sensing," *IEEE Transactions on Information Theory*, vol. 52, no. 4, pp. 1289–1306, April 2006.

[2] E. J. Candes, J. K. Romberg, and T. Tao, "Stable signal recovery from incomplete and inaccurate measurements," *Communications on pure and applied mathematics*, vol. 59, no. 8, pp. 1207–1223, 2006.

[3] D. Ramasamy, S. Venkateswaran, and U. Madhow, "Compressive Parameter Estimation in AWGN," *IEEE Transactions on Signal Processing*, vol. 62, no. 8, pp. 2012–2027, February 2014.

[4] K. Hyun and L. A. Gerhardt, "The use of laser structured light for 3D surface measurement and inspection," in *Proceedings of the Fourth International Conference on Computer Integrated Manufacturing and Automation Technology*, October 1994, pp. 215–221.

[5] O. Scholz, G. Kostka, A. Jobst, and P. Schmitt, "Laser Sheet of Light Measurement in Tire Manufacturing and Vehicle Assembly," in *SAE Technical Paper 2008-01-0231*, 2008.

[6] N. Vukašinović, M. Korošec, and J. Duhovnik, "The Influence of Surface Topology on the Accuracy of Laser Triangulation Scanning Results," *Journal of Mechanical Engineering*, vol. 56, no. 1, pp. 23–30, 2010.

[7] C. Norström, *Underwater 3-D imaging with laser triangulation*. Linköping: Master's Thesis, Tekniska Högskolan Linköpings Universitet, 2006.

[8] S. Slob and R. Hack, "3D Terrestrial Laser Scanning as a New Field Measurement and Monitoring Technique," in *Engineering Geology for Infrastructure Planning in Europe: A European Perspective*, vol. 104, 2004, pp. 179–189.

[9] H.-G. Maas, B. Hentschel, and F. Schreiber, "An optical triangulation method for height measurements on water surfaces," in *Videometrics VIII (Elec-tronic Imaging 2003), Ed. S. El Hakim, SPIE Proceedings*, vol. 5013, 2003, pp. 103–109.

[10] R. F. Marcia, Z. T. Harmany, and R. M. Willett, "Compressive coded aperture imaging," in *Proceedings of SPIE Electronic Imaging*, 2009, p. 72460.

[11] R. Robucci, J. D. Gray, L. K. Chiu, R. J, and P. Hasler, "Compressive sensing on a cmos separable-transform image sensor," *Proceedings of the IEEE*, vol. 98, no. 6, pp. 1089–1101, June 2010.

[12] R. M. Willett, R. F. Marcia, and J. M. Nichols, "Compressed sensing for practical optical imaging systems: a tutorial," *Optical Engineering*, vol. 50, no. 7, pp. 072 601–072 601–13, 2011.

[13] K. Fyhn, M. F. Duarte, and S. H. Jensen, "Compressive Parameter Estimation for Sparse Translation-Invariant Signals Using Polar Interpolation," *IEEE Transactions on Signal Processing*, vol. 63, no. 4, February 2015.

[14] M. B. Wakin, "Manifold-Based Signal Recovery and Parameter Estimation from Compressive Measurements," *Available: http://arxiv.org/abs/1002.1247, preprint*, 2010.

[15] D. K. Naidu and R. B. Fischer, "A Comparative Analysis of Algorithms for Determining the Peak Position of a Stripe to Subpixel Accuracy," in *Proceedings British Machine Vision Conference*, 1991, pp. 217–225.

[16] M. F. Duarte, M. A. Davenport, D. Takhar, J. N. Laska, T. Sun, K. F. Kelly, and R. G. Baraniuk, "Single-pixel imaging via compressive sampling," *IEEE Signal Processing Magazine*, vol. 25, no. 2, pp. 83–91, 2008.

[17] I. T. Young, J. J. Gerbrands, and L. J. van Vliet, *Fundamentals Of Image Processing*. Cip-data Koninklijke Bibliotheek, Den Haag, 1995.

[18] R. Willett and M. Raginsky, "Poisson Compressed Sensing," *Defense Applications of Signal Processing*, 2011.

[19] Z. T. Harmany, R. F. Marcia, and R. M. Willett, "This is SPIRAL-TAP: Sparse Poisson Intensity Reconstruction ALgorithms - Theory and Practice," *IEEE Transactions on Signal Processing*, vol. 21, no. 3, pp. 1084–1096, September 2011.